Hindawi
Advances in Civil Engineering
Volume 2019, Article ID 3546052, 12 pages
https://doi.org/10.1155/2019/3546052

Research Article

Experimental Study on the Deterioration Rules of Anchoring Performance of Rock Mass under Different Joints Distribution

Wantao Ding[1,2] **Minglei Hou**[2] **Lei Chen**[2] **Keqi Liu**[2] **Rui Chen**[2] **Yang Wang**[2] **and Mingbin Wang**[3]

[1]*Research Center of Geotechnical and Structural Engineering, Shandong University, Jinan 250061, China*
[2]*School of Qilu Transportation, Shandong University, Jinan 250002, China*
[3]*School of Civil Engineering, Ludong University, Yantai 264025, China*

Correspondence should be addressed to Wantao Ding; dingwantao@sdu.edu.cn

Received 31 July 2019; Accepted 20 September 2019; Published 21 October 2019

Academic Editor: Timo Saksala

In order to analyze the influence of damage caused by corrosion on anchoring performance of a rock mass with different joints, the anchored rock mass specimens with different joints distribution were prepared. An electrochemical accelerated corrosion test of specimens was carried out, and the mechanical test of them under different corrosion time was also investigated. The results showed that the pitting corrosion is the main form of the anchor bar corrosion of an anchoring rock mass with different joints, and the shape of the etch pit is reverse semi-ellipse. With the increase of pitting ratio, the ultimate bond strength and the corresponding slide distance decrease gradually. The effects of pitting ratio on the slide distance of the anchor bar in an anchored joint rock mass are insignificant, but these on the bond strength of it are significant. The bond-slide model of the anchored joint rock mass with different pitting ratios was established. The research results of this paper can provide reference for analyzing the corrosion damage of a complex anchored joint rock mass in practical engineering and a theoretical basis for the design optimization of anchoring support in the complex jointed rock mass.

1. Introduction

Anchorage system, as the key element of underground engineering structure, has gradually become the preferred method for the engineering reinforcement of rock slopes, tunnels, as well as in deep foundation pit and other projects [1–4]. Because of the complexity of the anchorage system itself, the difficulty of quality control, and its concealment during construction, corrosion becomes the key problem affecting the safety of the anchorage system [5]. At present, corrosion of the anchorage system is mainly caused by carbonization of grouting protective layer, erosion of acid medium, and induction of stray current [6–8]. Among them, the acidic media like chloride ion is the main reason for the deterioration of the durability of the anchorage system. Especially in submarine tunnels, the seepage of seawater provides sufficient oxygen and appropriate relative humidity for the corrosion. It can also accelerate the corrosion of the anchorage system, weaken the strength of jointed rock mass, and ultimately lead to premature failure of the anchorage system [9]. Thus, it is critical to investigate the corrosion effect of the anchorage system.

Recently, there are few studies on the durability of the anchorage system, but a large number of theoretical models [10], numerical simulations [11], and laboratory tests [12] have been carried out on the corrosion of steel bar in reinforced concrete structure. The effect of corrosion on the bond properties of reinforced concrete is the hot topic. Kemp et al. [13] studied the effect of different natural corrosion conditions on bond properties. It was found that the larger the diameter of steel bar is, the greater the promotion of corrosion on bonding properties is. However, the natural corrosion ratio is low, so the test results are not representative. Therefore, in order to accelerate the corrosion ratio of the steel bar, researchers began to use the electrochemical acceleration method to get the steel bar

specimens with a high corrosion ratio [14–16], although the geological environment of the anchorage system is more complicated than the concrete structure. Under the influence of ground stress, the stress state of the anchorage system is often affected by many uncertain factors. But with the high similarity between the anchorage system and reinforced concrete structure in composition material (steel bar and cement mortar) and corrosion mechanism, the research ideas and methods can be used for reference.

Extending the research region away from anchor system corrosion, there is some basic studies on the durability and safety of the anchorage system. Assisted with numerical methods, Ding et al. [17, 18] analyzed the effect of corrosion on the performance deterioration of the anchorage system. It can be found that the deformation of the bolting zone and the plastic zone of the surrounding rock increases gradually with the rise of the corrosion degree of rock bolt. Using the system reliability theory and the limit equilibrium analysis method, a direct method for the failure probability of the anchorage system of rock slope with double sliding blocks was proposed by Chen and Cheng [19]. In addition, the durability and safety of the anchorage system are also investigated through model tests, laboratory tests, and field tests. For instance, Qiu et al. [20] analyzed the mechanical characteristics of lining during the deterioration of initial support of deep-buried rocky tunnel by model test. It is concluded that the deterioration of bolt has more obvious influence on secondary lining than that of shotcrete. Gamboa and Atrens [6, 21] carried out the effect of corrosion on the anchorage system performance from two aspects of environment and materials through the stress corrosion cracking (SCC) test. Through laboratory tests, Zhao et al. [22] concluded that the chloride ion content in groundwater is the most important factor affecting the service life of bolts.

Anchorage performance of the jointed rock mass in geotechnical engineering is the key problem to be analyzed by numerous researchers. Griffith [23] first proposed the famous "Griffith fracture theory," which was later applied by Hoek [24] to study the strength characteristics of the jointed rock mass under biaxial pressure. Subsequently, the model test using gypsum as a similar material for the jointed rock mass has been gradually developed. The fracture failure shape of a single-jointed rock mass can be well described by uniaxial [25], biaxial [26], and triaxial compression tests [27], but it can only simulate the jointed rock mass under dry conditions. Making the cracked mortar specimens to simulate the semi-penetrating jointed rock mass, Ding et al. [28] obtained the calculation model of the corrosion amount under different loading time and proposed the formula of pitting ratio based on the concept of mass loss rate. In order to more accurately simulate the situation at the scene, Wu et al. [29] analyzed the SCC of full-scale anchor bars. In some studies, it has been found that the force exerted by the bolt is proportional to the interface of the bolt [30], and the shear strength of the joint surface is increased greatly. The diameter and inclination of bolt have a great influence on the shear displacement of the anchorage body [31, 32]. The larger the inclination of the bolt, the smaller the shear stress can be provided, and the optimum bolt mounting angle is present [33]. The prefabricated joints have a weakening effect on the strength, elastic modulus, and peak axial strain of the rock mass. The more joints there are, the more obvious the weakening effect will be [34].

In summary, some achievements have been made in the research on the degradation of bond properties caused by corrosion of the steel bar and the durability of anchor system, but there are relatively few studies on the corrosion damage of different anchored joints rock mass. And, many researchers investigate the anchored joint rock mass based on uniform corrosion, which is inconsistent with the actual situation. Based on the accelerated corrosion test of the anchored joint rock mass, the effect of pitting ratio under different joints distribution on the mechanical properties of anchorage system was studied. Corresponding to different pitting ratios, the relationships between slide ratio, ultimate bond strength, slide distance, and bond stress of anchorage system are studied, respectively. A bond-slide model of anchored rock mass specimens for different joints distribution was also established. These results can be used as a basis and reference for predicting the degradation of mechanical properties of different anchored joints rock mass.

2. Experimental Design

2.1. Preparation of Anchored Joint Rock Mass Specimens. In order to analyze the effect of corrosion degree under different joints distribution on the bond properties of the anchor system, six kinds of anchored rock mass specimens with different joints distribution are designed, which are semi-penetrating single-jointed rock mass specimens (group A), penetrating single-jointed rock mass specimens (group B), penetrating double-jointed rock mass specimens (group C), cross-semi-penetrating jointed rock mass specimens (group D), cross-penetrating jointed rock mass specimens (group E), and semi-penetrating double-jointed rock mass specimens (group F). At first, the original rock was used as the specimen, but after reducing the specimen in equal proportion, the scaled anchoring jointed rock mass specimens are difficult to operate, the anchor bar would cause great damage to the specimen, and the anchoring performance is not good. So, we use similar materials to simulate the original rock mass. According to previous research, we have chosen resin, concrete, and cement mortar as similar materials, but the permeability of resin and concrete is poor, and the permeability of cement mortar is consistent with the seabed surrounding rock. Therefore, by making mortar specimens with different mix ratios for cubic compressive strength test, the best mix ratio of cement mortar is selected, which has similar strength with the original rock mass. Compressive strength tests are carried out on each group of rock mass specimen with different joints distribution to ensure that their strength meets the test requirements.

The size of the specimen is 75 mm × 75 mm × 150 mm, and an HRB335 rebar with a diameter of 12 mm and a length of 170 mm is embedded in the center. The length of the rebar embedded in the mortar specimen is 120 mm, while the length of the rebar exposed outside is 50 mm. There is a 30 mm mortar protective layer at the bottom of the

specimen. The size and joint distribution of specimens are shown in Figure 1. Semi-penetrating joints and penetrating joints are simulated by thin iron sheets in the mold (Figure 2). The joint is at 45° to the horizontal, and the corresponding sizes are 75 mm × 37.5 mm × 1 mm and 75 mm × 7.5 mm × 1 mm, respectively.

The cement used in the experiment is ordinary Portland cement, grade 42.5, produced by Sunnsy Group. The sand is produced in Jiyang, Jinan. Purified water and the retarding efficient water reducing agent, UNF-3A, are also used in the preparation of specimens, and the corresponding mix proportion of mortar quality is shown in Table 1. After pouring the specimens into the standard curing room for 28 days, the average measured compressive strength of the standard cube specimen, with the size of 150 mm × 150 mm × 150 mm is 60.87 MPa as shown in Figure 3, which meets the strength requirements of the experiment.

2.2. Corrosion of Anchored Joint Rock Mass Specimens. In practical engineering, though the anchor bar of the anchored joint rock mass directly connects with the seawater because of joints, corrosion of the anchor bar may still need an extremely long time. Based on the choice of the test cycle, more researchers will adopt an accelerated corrosion test. At present, there are two kinds of accelerated corrosion tests, one is to create a more easily corroded environment to accelerate corrosion (such as regular spraying of saltwater), and the other is to directly electrify the anchor bar to accelerate corrosion. Although the corrosion of anchor bar simulated by the first method is more realistic and the test conditions are simpler and easier to operate, the corrosion time is much longer than that of the second method, and the quantitative control of corrosion can not be carried out in the operation process. The second method is more accepted and adopted by researchers. The wet-electrification method (in the process of accelerated corrosion by electrification, the sample is immersed in seawater to form an electrolytic cell, and chloride ions will accelerate the corrosion of sample) is widely used because of its fast corrosion speed, short test period, and the quantitative calculation of the quality of corrosion products (theoretical mass value) by Faraday's law. Therefore, DC-regulated power supply, PS-6005D-II, is used to accelerate corrosion in this experiment. The two-electrode system was applied in the experiment, i.e., exposed anchor bars are used as anodes to connect DC power supply, and copper sheets are used as cathodes to connect DC power supply. The accelerating corrosion device is shown in Figure 4. In order to simulate the natural corrosion environment of seawater, the electrolyte was taken from the Yellow Sea of Qingdao. The results of seawater composition test are shown in Table 2. The specimens are immersed in the electrolyte with the current of 50 mA. The electrolyte should be added continuously during the acceleration process of corrosion to ensure that the specimens can fully contact with the electrolyte. In this experiment, 10 different accelerated corrosion times were designed for each group of specimens to control pitting ratio, which were 0 h (no corrosion), 24 h, 36 h, 48 h, 60 h, 72 h, 84 h, 96 h, 108 h, and 120 h, respectively.

2.3. Experimental Design of Bond Properties. According to the requirements of *Standard for Test Method of Concrete Structures* (*GB/T 50152-2012*), there are four common methods to analyze the bond properties: central tension test (the test operation is difficult), beam test (large specimen size and high production cost), column test (specimen fabrication, data acquisition, and analysis are complicated.), and central pull-out test. The central pull-out test specimens are usually prisms or cubes, which are easy to fabricate. When pouring specimens, the anchor bars are buried in the center of the specimens. The bare anchor bar on one side is easy to clamp when loading the specimen, but the other side needs the help of the reaction frame. The reaction frame is composed of two iron plates and four pillars. The top iron plate connects with the chuck, and the bottom of the chuck is a spherical hinge, which can ensure that the specimen will not be subject to eccentric force during the experiment. This method is characterized by simple specimen preparation, easy operation, and lower cost. In addition, this method can simulate the load slip of the anchor bar and the bond-slip relationship between the anchor bar and mortar. The theory is clear, and it is sensitive to the change of the appearance characteristics of the anchor bar. It is a benchmark method for evaluating the bond performance of the anchored rock mass.

The hydraulic universal testing machine, WDW-IOOE III, is used in the loading test. The maximum tensile force exerted by the testing machine is 100 kN, as shown in Figure 5. In order to analyse the "whole process" failure condition of specimens, the displacement of the chuck on the test machine was controlled at a speed of 1 mm/min by the continuous monotone loading method until the specimen was destroyed.

3. Analysis of Test Results

3.1. Corrosion Shape Analysis of Anchored Joint Rock Mass. In the laboratory test, the anchored joint rock mass specimens are directly immersed in the electrolyte, which is seawater. The corrosion of anchor bar develops radially and axially, as shown in Figure 6.

The etch pit shape of the anchor bar opens upward, which is contrary to the semi-elliptic model proposed by Liu [35]. Therefore, the distribution model of corrosion amount is established based on ellipsoid shape, which is similar to the shape of the anchor bar after corrosion. The maximum depth of the corrosion pit is d_a, the maximum thickness of the corrosion products after expansion is d_m, and the approximate model is shown in Figure 7.

It can be seen from Figure 7 that the mass of the corrosion products consist of two parts. One part is M_t, which is the mass of the corrosion products filled in the range of the

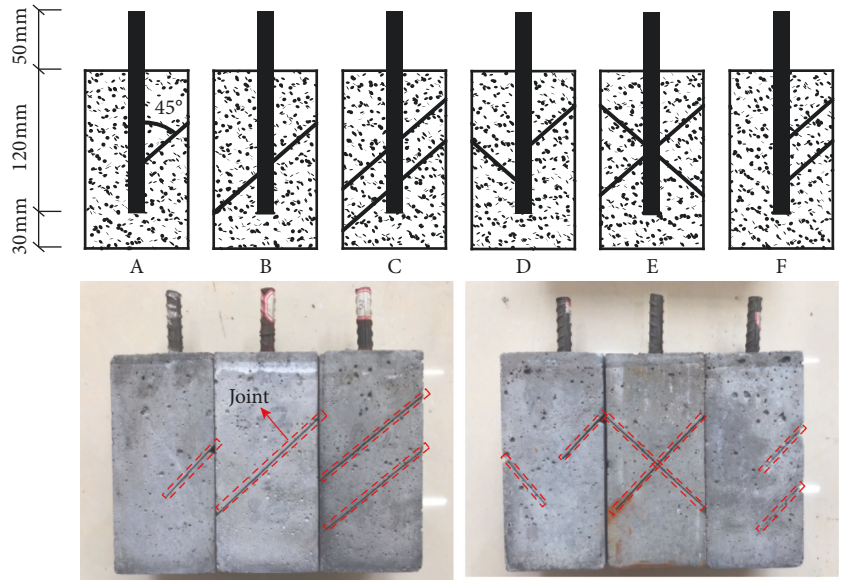

Figure 1: Size and joint distribution of specimens.

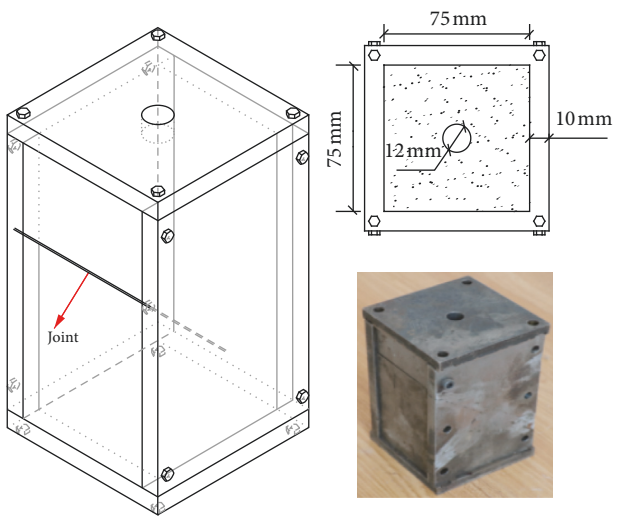

Figure 2: Experimental mold.

etch pit. The other part is M_k, which is the mass of the corrosion products expanded outside of the etch pit. The total corrosion amount, M_z, can be expressed as follows:

$$M_z = M_t + M_k. \tag{1}$$

Taking the cross-section of the corroded anchor bar of unit length for analysis, the mass of corrosion products in each part can be expressed as follows:

$$M_t = \rho_x \cdot \left[\frac{R^2}{2}(\pi - 2\theta) - 2(R - d_a)R\cos\theta\right], \tag{2}$$

$$M_k = \rho_x\left[\frac{\pi}{2}\cdot R\cdot(R + d_m) - \frac{\pi}{2}R^2\right] = \frac{\pi\rho_x}{2}Rd_m, \tag{3}$$

where ρ_x is the density of corrosion products, g/mm^3; R is the radius of anchor, mm; and θ is the polar angle.

As can be seen from the literature [36], the mass of corrosion products is obtained as follows:

$$M_t = \alpha_{rust}M_z\frac{\rho_x}{\rho'}, \tag{4}$$

where α_{rust} is the mass ratio between anchor bar and its corrosion products, which generally takes the values between 0.523 and 0.622 and ρ' is the density of the anchor bar, g/mm^3.

From equations (2) and (4), we obtain the equation for d_a as

$$d_a = \frac{M_z\alpha_{rust}}{4R\rho\cos\theta} - \frac{R(\pi - 2\theta)}{4\cos\theta} + R. \tag{5}$$

From equations (2), (3), and (4), we obtain the equation for d_m:

$$d_m = \frac{2M_z}{\pi R\rho_x} - \frac{2M_z\alpha_{rust}}{\pi R\rho}. \tag{6}$$

The shape of the etch pit would not be so regular in the actual engineering, there is a certain error in the approximate semicircular model of the etch pit area. In addition, when calculating the M_t, the uncorroded anchor bar is reduced to a triangle, which is different from the actual triangular shape with a circular arc. Therefore, the distribution model of corrosion amount proposed in this paper can be used as a simplified computing model.

Pitting corrosion is the primary form of the anchor bar corrosion in this test. With the rapid development and expansion of anchor bar corrosion under the influence of constant current, most of the corrosion products will overflow from the position of joint, and a concave etch pit will be finally formed. Moreover, corrosion will diminish the bond properties of the anchor bar and the overall anchoring performance. Since the length of the anchor section is longer, the corrosion ratio is smaller under the same amount of corrosion. It is not accurate

Table 1: Mix proportion of mortar quality.

Cement (g)	Dinas (g)				Water (g)	Water-reducer (g)
	10~20 meshes	20~40 meshes	40~70 meshes	70~120 meshes		
1000	1247	625	311	157	350	20

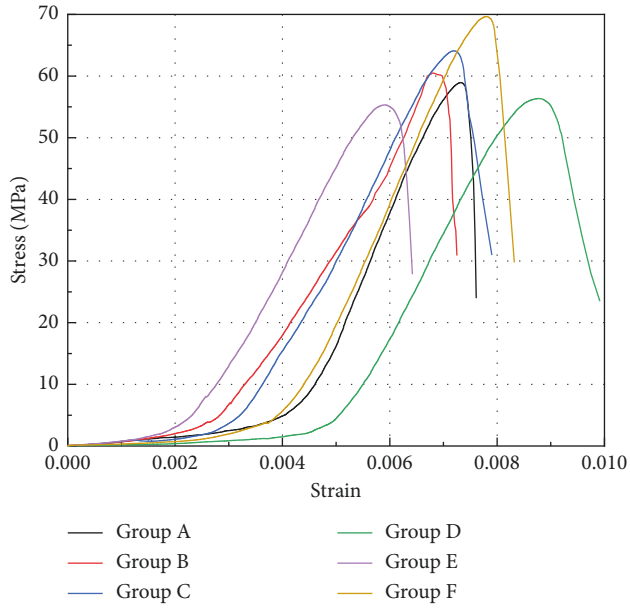

Figure 3: Stress-strain curve of uniaxial compression.

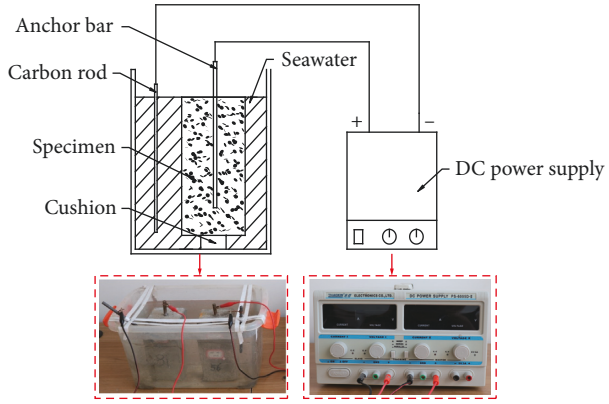

Figure 4: Accelerated corrosion device.

Table 2: Factor loading matrix.

Ion	Concentration (mg/L)
Calcium ion (Ca^{2+})	431
Magnesium ion (Mg^{2+})	1348
Sodium ion (Na^{+})	11458
Potassium ion (K^{+})	421
Chloride ion (Cl^{-})	17345
Sulfate ion (SO_2^{-4})	2539
Bicarbonate ion (HCO_3^{-})	160
Nitrate ion (NO_3^{-})	4

to calculate the corrosion ratio based on the total mass loss of the anchor section. Therefore, we use the concept of pitting ratio [37], which can be calculated as follows:

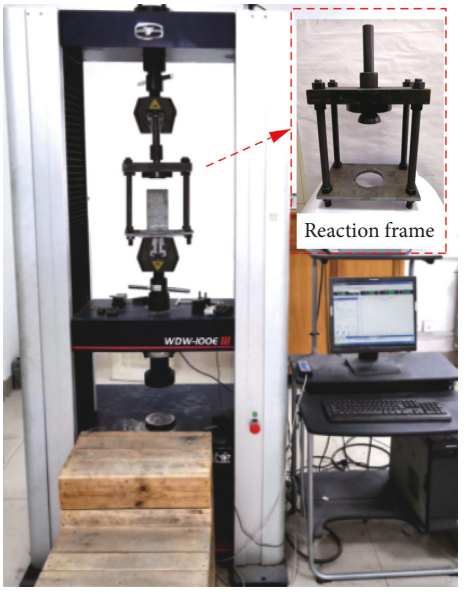

Figure 5: Experimental device of central pull-out test.

$$\eta = \frac{m_0 - m_c}{m_0}, \tag{7}$$

$$m_0 = \rho \pi R^2 b, \tag{8}$$

where η is the pitting ratio, m_0 is the original mass of the anchor bar before pitting corrosion, m_c is the mass of the

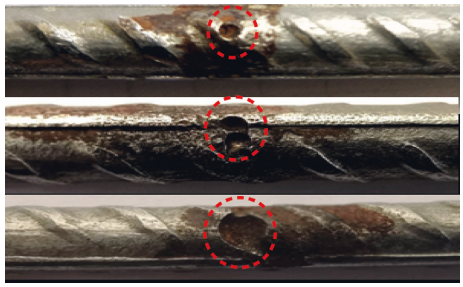

Figure 6: Shape of the etch pit.

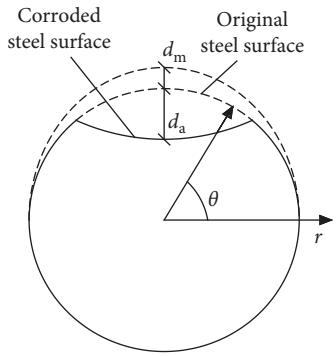

Figure 7: The reverse semi-elliptic model.

anchor bar after pickling, and b is the corrosion length along the direction of the anchor bar.

3.2. Analysis of the Relationship between Slide Distance and Bond Stress. In the test, the universal testing machine automatically records the drawing force and the total slide distance of the anchor bar during the central pull-out test. It is assumed that the bond stress, τ, is uniformly distributed along the cross-section of the anchor bar, and the tensile deformation of the anchor bar meets the Hooke's law. The bond stress, τ, and the slide distance, S, of the anchor bar can be calculated by the equations (9) and (10). The area diagram of the subtracted part is shown in Figure 8.

$$\tau = \frac{P}{\pi d l_a - (1/2)\pi d l_0}, \tag{9}$$

$$S = S_a - \frac{F}{EA} L_{AB}, \tag{10}$$

$$l_0 = \frac{h_0}{\sin \varphi}, \tag{11}$$

where P is the loading of the central pull-out test, kN; d is the diameter of anchor bar, mm; l_a is the length of anchor bar, mm; l_0 is the length of anchor bar which directly contacts with seawater, mm; S_a is the total distance of the slide, mm; L_{AB} is the original length of the anchor bar, mm; A is the theoretical area of cross-section of the anchor bar, mm^2; E is the elastic modulus, MPa; F is the maximum loading of the central pull-out test, kN; h_0 is the width of joints, mm; and φ is the dip angle of the joints.

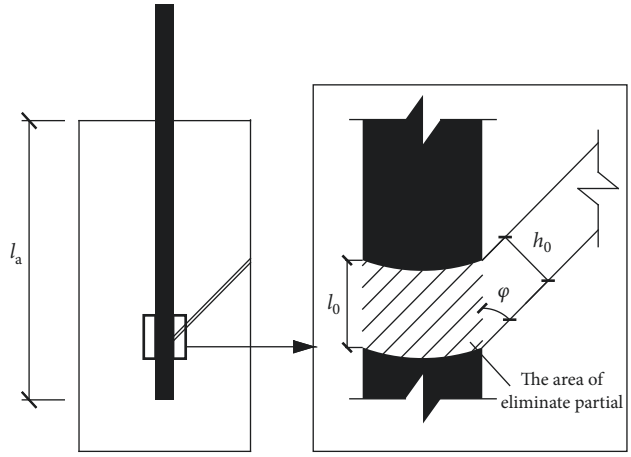

Figure 8: Schematic diagram of the calculating area.

Based on the six kinds of anchored rock mass specimens with different joints distribution, the relationship between slide distance and bond stress is analyzed. Due to space limitation, the experimental results of group A are shown in Figure 9.

Figure 9 shows that the first stage is at the beginning of the test, and the bond stress is 65%–73% of the ultimate bond stress, at which the slope of the curve is large. When the bond stress is further increased to the ultimate bond stress, the slope of the curve decreases gradually, which is the second stage. This indicates that the shear stiffness of the anchoring section of the first stage is greater than that of the second stage. Because the volume of the anchor bar after corrosion is larger than the original volume, which will cause compressive stress on the surrounding rock. The friction between the anchor bar and the specimen will increase. Furthermore, the anchoring capacity of the anchor bar will also raise. With the continuation of the test, the chemical gumming force between the anchor bar and the surrounding rock is gradually destroyed. At this time, the bonding force mainly depends on the friction force and mechanical biting force between them. Subsequently, the compressive stress of the anchor bar on the surrounding rock increases gradually, and the influence of corrosion degree of the anchor bar on bonding force becomes more and more obvious with the development of surrounding rock joints. Before the failure of specimens, the slide distance increases slowly with the increase of bond stress, and there is a linear relationship between them. Moreover, the slope of the first stage slows down gradually with increasing pitting ratio. This is because the chemical gumming force between the anchor bar and surrounding rock is destroyed along the longitudinal direction with increasing pitting ratio, which reduces the bond strength on the first stage.

3.3. Analysis of the Relationship between Pitting Ratio and Ultimate Bond Strength. By comparing the ultimate bond strength of each group, the relationship between the pitting ratio and the ultimate bond strength is shown in Figure 10.

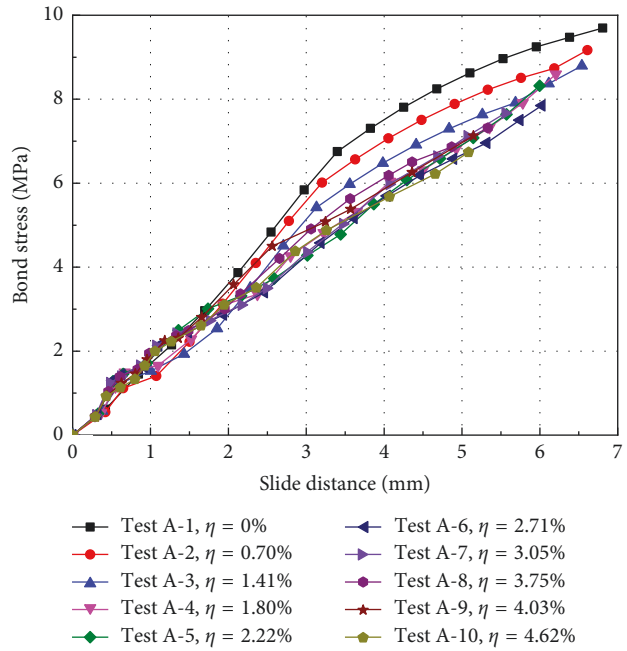

Figure 9: The relationship between bond stress and slide distance obtained in group A.

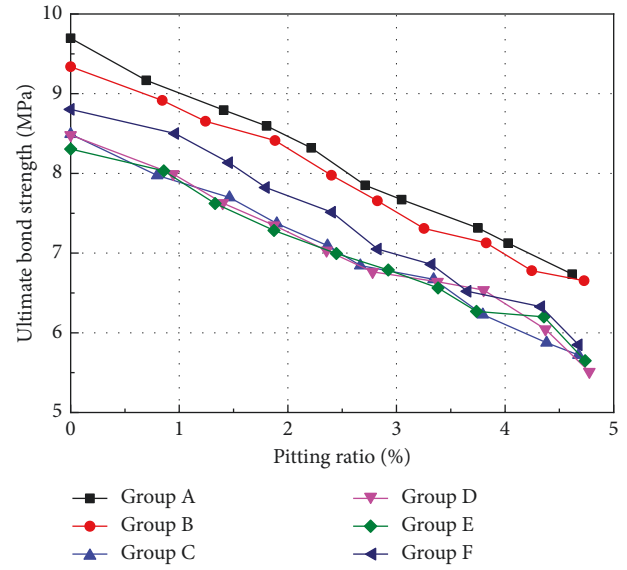

Figure 10: The relationship between pitting ratio and ultimate bond strength.

From Figure 10, it can be seen that the pitting ratio has a negative linear correlation with the ultimate bond strength. At the initial stage of corrosion, the bond strength did not increase because of the volume expansion of corrosion products. However, as the volume of corrosion products expands continuously, cracks may appear in the specimens, which reduce the anchoring capacity and ultimate bond strength.

In group A, the ultimate bond strength is about 9.695 MPa without corrosion. When pitting ratio reaches 4.62%, the value is 6.735 MPa, and the ultimate bond strength is decreased by 30.53%. The ultimate bond strength of groups B, C, D, E, and F decreased by 28.76%, 32.63%, 35.02%, 31.99%, and 33.56%, respectively. It can be seen that the overall change trend of each group is the same, but there are differences in the test results of different groups. By comparing group A (single joint) with group F (double joint), it can be seen that the effect of pitting corrosion on bond strength is more obvious with the increase of joints, that is, the more joints there are, the more serious the corrosion is, and the deterioration of bond mechanical properties of anchorage system is obvious. This can be verified by group B (single joint) and group C (double joint). Moreover, comparing the test data of the anchored joint rock mass specimens with semi-penetrating joints with that of penetrating joints, notice that the bond strength decreases gradually with the increase of contact area between the seawater and anchored bar for the specimens of groups A, B, C, and F under the same pitting ratio, and the joints in the specimens of groups A, B, C, and F are on the same side; the effect on the bond strength is insignificant with increasing the contact areas for the specimens of groups D and E under the same pitting ratio, and the joints in the specimens of groups D and E intersect with each other.

The reduction factor of ultimate bond strength, δ, can be defined as the ratio of the ultimate bond strength between the anchor bar of different pitting ratios and uncorroded anchor bar in the same group of tests.

$$\delta = \frac{\tau_i}{\tau_0}, \tag{12}$$

where τ_i is the ultimate bond strength at different pitting ratios, MPa, and τ_0 is the ultimate bond strength without corrosion, MPa.

Equation (12) shows that the ultimate bond strength at any pitting ratio can be obtained from the ultimate bond stress strength without corrosion. The relationship between the ultimate bond strength reduction factor and the pitting ratio is shown in Figure 11.

Fitting the experimental data in Figure 11, the equation between δ and η can be obtained. The coefficient of determination values, R^2, are all close to 1, showing a good fit.

$$\delta = \begin{cases} 0.998 - 6.574\eta, & (R^2 = 0.996), \\ 1.006 - 6.419\eta, & (R^2 = 0.991), \\ 1.000 - 6.945\eta, & (R^2 = 0.994), \\ 0.999 - 6.764\eta, & (R^2 = 0.976), \\ 1.007 - 6.536\eta, & (R^2 = 0.984), \\ 1.020 - 7.330\eta, & (R^2 = 0.984). \end{cases} \tag{13}$$

3.4. Analysis of Relationship between Pitting Ratio and Slide Distance. The slide distance corresponding to the ultimate bond strength in each group of tests is analyzed. The relationship between the slide distance and pitting ratio is shown in Figure 12.

Figure 12 shows that the slide distance gradually decreases as the pitting ratio increases. In group A, the slide

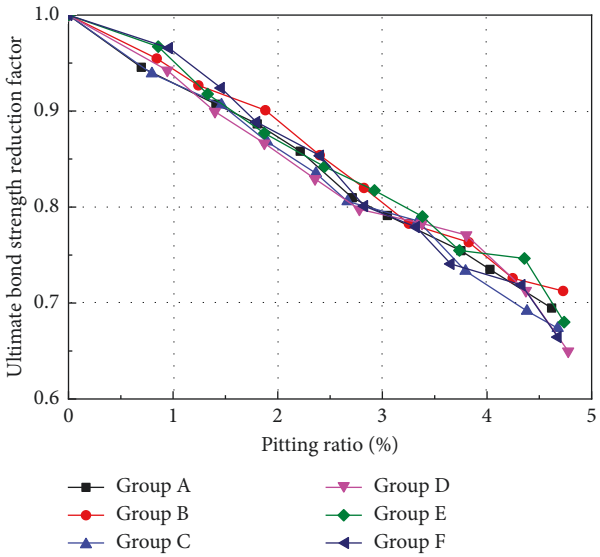

Figure 11: The relationship between the pitting ratio and bond strength reduction factor.

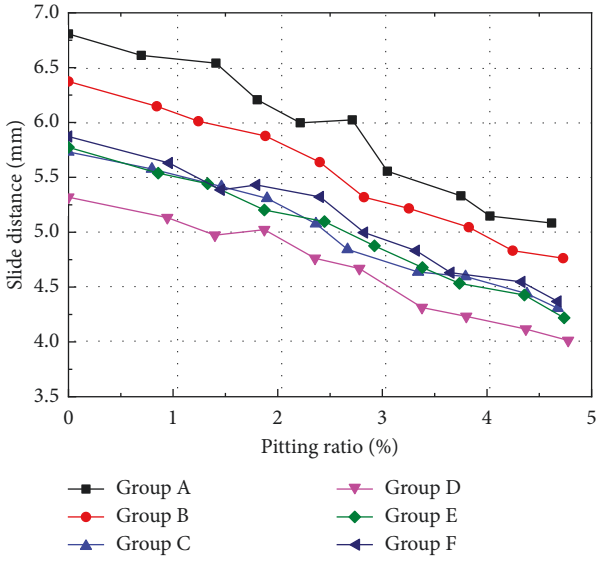

Figure 12: The relationship between pitting ratio and slide distance.

distance of the anchor bar without corrosion is 6.808 mm. When pitting ratio reaches 4.62%, the value is 5.084 mm, which decreases by 25.32%. The slide distance of groups B, C, D, E, and F decreased by 25.27%, 24.86%, 24.55%, 26.93%, and 25.61%, respectively. It can be seen that the change of slide distance with the pitting ratio is similar in each group, that is, the total relationship of anchor bar corrosion with different joints distribution tends to be consistent. However, the slide distance of the groups A, D, and F is slightly increased when the pitting ratio is 1.4% to 2.8%. This is because, for the semi-penetrating jointed rock mass specimens, the rock mass connecting with the anchored bar at the effect range of joints plays a role of protecting the anchored bar. With the increase of the number of semi-penetrating joints, the protective effect caused by the rock mass connecting with the anchored bar will occur in the low pitting ratio.

The slide ratio can be defined as the ratio of the slide distance corresponding to the ultimate bond strength between the anchor bar of different pitting ratios and uncorroded anchor bar in the same group of tests.

$$\varepsilon = \frac{S_i}{S_0}, \tag{14}$$

where ε is the slide ratio; S_i is the slide distance corresponding to the ultimate bond strength at different pitting ratios, mm; and S_0 is the slide distance corresponding to ultimate bond strength without corrosion, mm.

The relationship between the slide ratio and pitting ratio is shown in Figure 13.

Fitting the experimental data according to the first-order exponential decay curve, we can obtain equation (15), which also shows a good fit.

$$\varepsilon = \begin{cases} e^{-5.915\eta} & (R^2 = 0.933), \\ e^{-6.009\eta} & (R^2 = 0.971), \\ e^{-5.771\eta} & (R^2 = 0.962), \\ e^{-5.534\eta} & (R^2 = 0.945), \\ e^{-6.089\eta} & (R^2 = 0.978), \\ e^{-5.828\eta} & (R^2 = 0.947). \end{cases} \tag{15}$$

4. Bond-Slide Model of Anchored Joint Rock Mass

In this test, the specimen was not arranged with stirrups, and the transverse rib of the anchor bar acts on the specimens to generate the hoop tensile stress, which eventually led to longitudinal splitting cracks. After reaching the peak stress, the specimen is split into several pieces, and the anchor bar is pulled out immediately because of the loss of clamping. Therefore, there is no descending stage and residual stage in the test [38]. It can be seen from Figure 4 that the distinction between microslide section and slide section is not obvious with increasing pitting ratio. However, the development of splitting section is more obvious with the increase of stress. Therefore, the experimental data can be linearly fitted in two stages. Taking group A as an example, the points on the bond-slide curve of the uncorroded specimen are fitted, which is shown in Figure 14.

By fitting the data for each group, the equation between τ_0 and S_0 can be obtained as shown in equations (16) to (21):

$$\tau_0 = \begin{cases} 1.906S_0, \\ 4.091 + 0.856S_0, \end{cases} \tag{16}$$

$$\tau_0 = \begin{cases} 1.961S_0, \\ 3.941 + 0.880S_0, \end{cases} \tag{17}$$

$$\tau_0 = \begin{cases} 1.944S_0, \\ 3.584 + 0.890S_0, \end{cases} \tag{18}$$

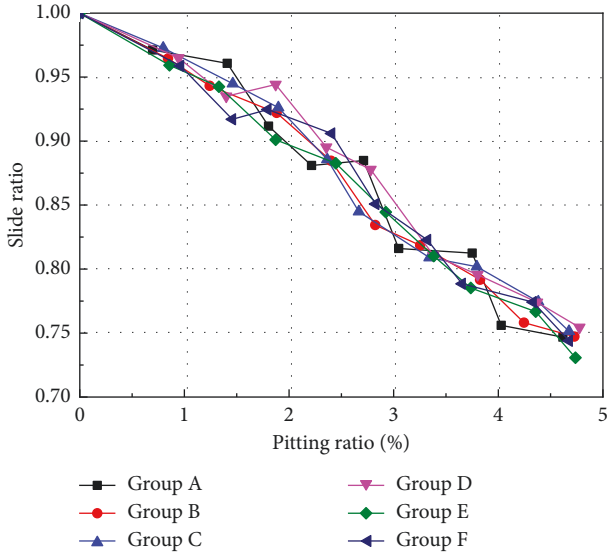

Figure 13: The relationship between the pitting ratio and slide ratio.

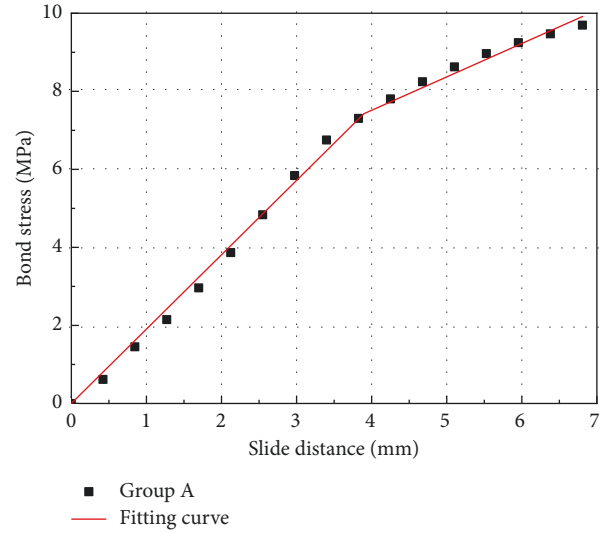

Figure 14: The bond-slide fitting curve of the uncorroded specimen in group A.

$$\tau_0 = \begin{cases} 2.134S_0, \\ 3.894 + 0.889S_0, \end{cases} \tag{19}$$

$$\tau_0 = \begin{cases} 1.925S_0, \\ 3.814 + 0.802S_0, \end{cases} \tag{20}$$

$$\tau_0 = \begin{cases} 2.006S_0, \\ 4.042 + 0.835S_0. \end{cases} \tag{21}$$

Introducing the equations (14) and (15) to the above equation, the equation of the bond-slide curves with different pitting ratios of each group can be obtained as shown in equations (22) to (27):

$$\tau_i = \begin{cases} (1.902 - 12.530\eta) \cdot S_i \cdot e^{5.915\eta}, \\ 4.083 - 26.894\eta + (0.854 - 5.627\eta) \cdot S_i \cdot e^{5.915\eta}, \end{cases} \tag{22}$$

$$\tau_i = \begin{cases} (1.973 - 12.588\eta) \cdot S_i \cdot e^{6.009\eta}, \\ 3.965 - 25.297\eta + (0.885 - 5.649\eta) \cdot S_i \cdot e^{6.009\eta}, \end{cases} \tag{23}$$

$$\tau_i = \begin{cases} (1.944 - 13.501\eta) \cdot S_i \cdot e^{5.771\eta}, \\ 3.584 - 24.891\eta + (0.890 - 6.181\eta) \cdot S_i \cdot e^{5.771\eta}, \end{cases} \tag{24}$$

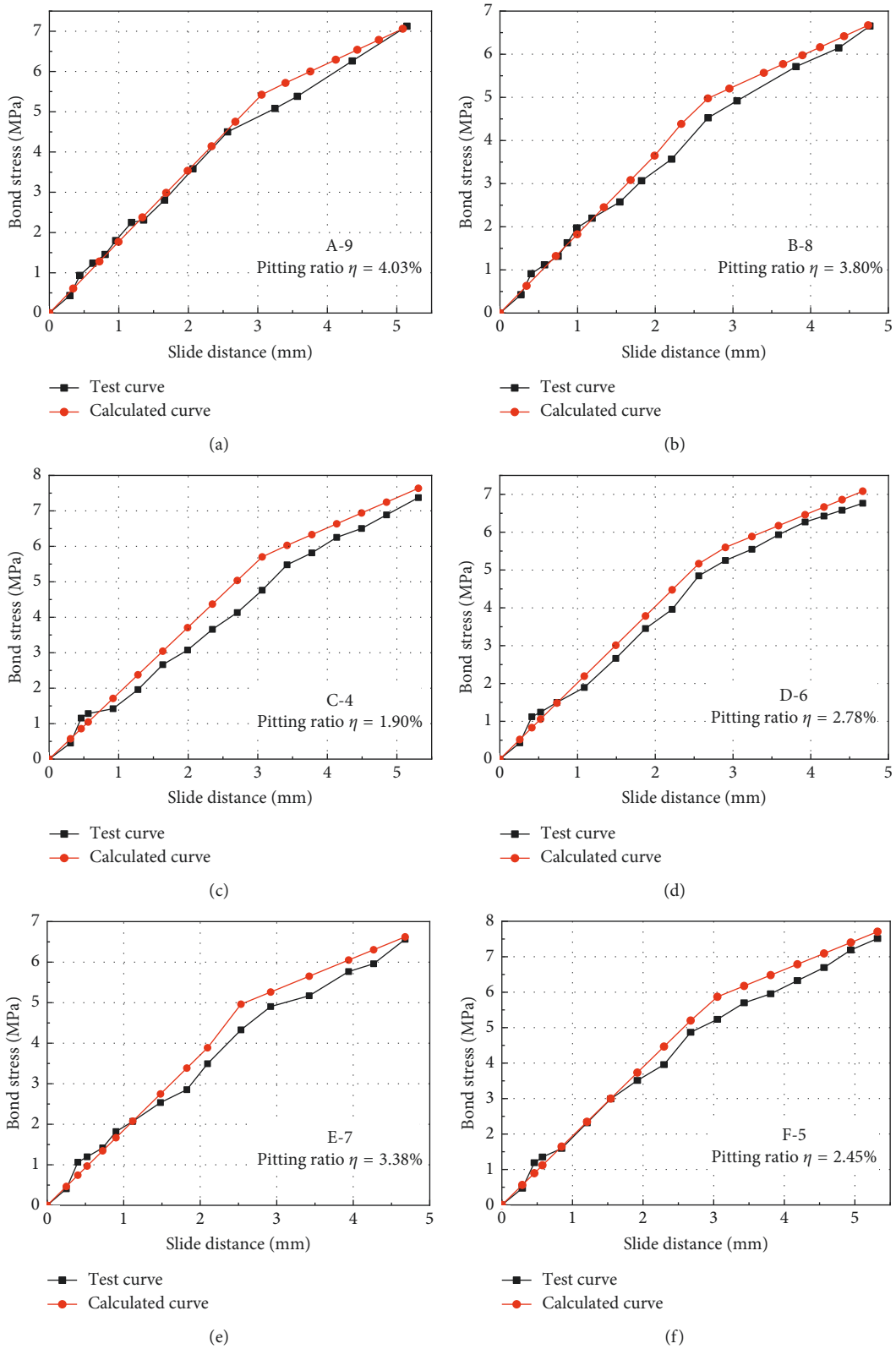

Figure 15: Comparisons between calculated results and test results of the bond-slide curve.

$$\tau_i = \begin{cases} (2.132 - 14.434\eta) \cdot S_i \cdot e^{5.534\eta}, \\ 3.890 - 26.339\eta + (0.888 - 6.013\eta) \cdot S_i \cdot e^{5.534\eta}, \end{cases} \quad (25)$$

$$\tau_i = \begin{cases} (1.938 - 12.582\eta) \cdot S_i \cdot e^{6.089\eta}, \\ 3.841 - 24.928\eta + (0.808 - 5.242\eta) \cdot S_i \cdot e^{6.089\eta}, \end{cases} \quad (26)$$

$$\tau_i = \begin{cases} (2.046 - 14.704\eta) \cdot S_i \cdot e^{5.828\eta}, \\ 4.123 - 29.628\eta + (0.852 - 6.121\eta) \cdot S_i \cdot e^{5.828\eta}. \end{cases} \quad (27)$$

Some test data were used to verify the equation of bond-slide curves with different pitting ratios. The calculated results were in good agreement with the test results, as shown in Figure 15.

5. Conclusion

In this paper, the anchorage performance tests of the anchored joint rock mass under different pitting ratios are carried out. The conclusions are as follows:

(1) Because the anchored joint rock mass specimens are directly immersed in the seawater, the corrosion firstly occurs at the position of the joints connecting with the anchored bar and then develops radially and axially. The etch pit opening is upward, and the shape of which is reverse semi-ellipse.

(2) With the increase of the number of joints, the influence of pitting ratio on bond strength becomes significant, that is, the more the number of joints under the same pitting ratio, the greater the decrease of the bond strength. Moreover, under the same pitting ratio, the bond strength decreases with the expansion of the joint range on the same side. For cross joints, the range of joints under the same pitting ratio has little effect on bond strength.

(3) For the semi-penetrating joint rock mass specimens, the rock mass connecting with the anchored bar at the effect range of joints plays a role of protecting the anchored bar. With the increase of the number of semi-penetrating joints, the protective effect caused by the rock mass connecting with the anchored bar will occur in the low pitting ratio.

(4) Compared with the slide distance before corrosion, the slide distance after corrosion of each group of the anchor bar is reduced about 25%. It can be seen that the changing trend of slide distance with pitting ratio is similar in each group, and there is no significant difference with the different distribution of joints.

(5) Based on the bond-slide model of the uncorroded anchored joint rock mass, the model is established by introducing the slide ratio and the reduction factor of ultimate bond strength of the corresponding models under different pitting ratios, which can reflect the deterioration rules of the anchoring mechanical properties of the anchored joint rock mass under different pitting ratios.

Data Availability

The data used to support the findings of this study are available from the corresponding author upon request.

Conflicts of Interest

The authors declare that they have no conflicts of interest.

Acknowledgments

The authors acknowledge the financial support provided by the National Natural Science Foundation of China (grant no. 41572275), the Natural Science Foundation of Shandong Province (grant no. ZR2018MEE051), and the Project of Shandong Province Higher Educational Science and Technology Program (grant no. J15LG01).

References

[1] S.-H. Jiang, D.-Q. Li, L.-M. Zhang, and C.-B. Zhou, "Time-dependent system reliability of anchored rock slopes considering rock bolt corrosion effect," *Engineering Geology*, vol. 175, pp. 1–8, 2014.

[2] R. R. Osgoui and E. Ünal, "An empirical method for design of grouted bolts in rock tunnels based on the geological strength index (GSI)," *Engineering Geology*, vol. 107, no. 3-4, pp. 154–166, 2009.

[3] S. Divi, D. Chandra, and J. Daemen, "Corrosion susceptibility of potential rock bolts in aerated multi-ionic simulated concentrated water," *Tunnelling and Underground Space Technology*, vol. 26, no. 1, pp. 124–129, 2011.

[4] Ö. Aydan, *Rock Reinforcement and Rock Support*, CRC Press, London, UK, 2018.

[5] P. P. Xanthakos, *Ground Anchors and Anchored Structures*, John Wiley & Sons Inc., New York, NY, USA, 1991.

[6] E. Gamboa and A. Atrens, "Environmental influence on the stress corrosion cracking of rock bolts," *Engineering Failure Analysis*, vol. 10, no. 5, pp. 521–558, 2003.

[7] H. Kang, Y. Wu, F. Gao, J. Lin, and P. Jiang, "Fracture characteristics in rock bolts in underground coal mine roadways," *International Journal of Rock Mechanics and Mining Sciences*, vol. 62, pp. 105–112, 2013.

[8] D. G. Karalis, N. E. Melanitis, and D. I. Pantelis, "Failure analysis of a rock anchor made of stainless steel in marine environment," *Engineering Failure Analysis*, vol. 19, pp. 123–130, 2012.

[9] T.-B. Zhao, W.-Y. Guo, Y.-L. Tan, C.-P. Lu, and C.-W. Wang, "Case histories of rock bursts under complicated geological conditions," *Bulletin of Engineering Geology and the Environment*, vol. 77, no. 4, pp. 1529–1545, 2018.

[10] L. Chernin, D. V. Val, and K. Y. Volokh, "Analytical modelling of concrete cover cracking caused by corrosion of reinforcement," *Materials and Structures*, vol. 43, no. 4, pp. 543–556, 2010.

[11] S. F. U. Ahmed, M. Maalej, and H. Mihashi, "Cover cracking of reinforced concrete beams due to corrosion of steel," *ACI Materials Journal*, vol. 104, no. 2, pp. 153–161, 2007.

[12] K. Zandi Hanjari, P. Kettil, and K. Lundgren, "Analysis of mechanical behavior of corroded reinforced concrete

structures," *ACI Structural Journal*, vol. 108, no. 5, pp. 532–541, 2011.

[13] E. L. Kemp, F. S. Brezny, and J. A. Unterspan, "Effect of rust and scale on the bond characteristics of deformed reinforcing bars," *Journal Proceedings*, vol. 7, no. 4, pp. 743–756, 1968.

[14] G. J. Al-Sulaimani, M. Kaleemullah, and I. A. Basunbul, "Influence of corrosion and cracking on bond behavior and strength of reinforced concrete members," *Structural Journal*, vol. 87, no. 2, pp. 220–231, 1990.

[15] E. Sola, J. Ožbolt, G. Balabanić, and Z. M. Mir, "Experimental and numerical study of accelerated corrosion of steel reinforcement in concrete: transport of corrosion products," *Cement and Concrete Research*, vol. 120, pp. 119–131, 2019.

[16] D. W. Law and T. C. K. Molyneaux, "Impact of corrosion on bond in uncracked concrete with confined and unconfined rebar," *Construction and Building Materials*, vol. 155, pp. 550–559, 2017.

[17] W.-T. Ding and S.-C. Li, "Effect of corrosion on reinforcement performance of anchorage support structure of subsea tunnel," *Journal of South China University of Technology*, vol. 41, no. 6, pp. 100–107, 2013.

[18] W.-T. Ding, J.-H. Liu, and L.-W. Zhang, "Analysis on interaction of rock-bolts in anchorage support structure of subsea tunnel at different corrosion levels," *Journal of Central South University*, vol. 45, no. 5, pp. 1642–1652, 2014.

[19] C.-F. Chen and X.-W. Cheng, "Time-varying reliability analysis of anchor system of rock slopes with double slide blocks," *Rock and Soil Mechanics*, vol. 33, no. 1, pp. 197–203, 2012.

[20] W.-G. Qiu, J.-M. Feng, X.-F. Chen, and H. Wang, "Model testing research on lining mechanical variation with deterioration process of primary support in deep hard rock tunnel," *Chinese Journal of Rock Mechanics and Engineering*, vol. 32, no. 1, pp. 72–77, 2013.

[21] E. Gamboa and A. Atrens, "Material influence on the stress corrosion cracking of rock bolts," *Engineering Failure Analysis*, vol. 12, no. 2, pp. 201–235, 2005.

[22] J. Zhao, W.-Z. Ji, L. Xiao et al., "In-situ experimental study on anchor durability," *Chinese Journal of Rock Mechanics and Engineering*, vol. 25, no. 7, pp. 1377–1385, 2006.

[23] A. A. Griffith, "The phenomena of rupture and flow in solids," *Philosophical Transactions of the Royal Society of London*, vol. 221, pp. 163–198, 1920.

[24] E. Hoek, *Rock Fracture under Static Stress Conditions*, Ph.D thesis, University of Cape Town, Cape Town, South Africa, 1965.

[25] B. Shen, O. Stephansson, H. H. Einstein, and B. Ghahreman, "Coalescence of fractures under shear stresses in experiments," *Journal of Geophysical Research: Solid Earth*, vol. 100, no. B4, pp. 5975–5990, 1995.

[26] A. Bobet and H. H. Einstein, "Fracture coalescence in rock-type materials under uniaxial and biaxial compression," *International Journal of Rock Mechanics and Mining Sciences*, vol. 35, no. 7, pp. 863–888, 1998.

[27] E. T. Brown, "Strength of models of rock with intermittent joints," *Journal of Soil Mechanics & Foundations Division*, vol. 96, no. 6, pp. 1935–1949, 1970.

[28] W.-T. Ding, M.-J. Li, M.-B. Wang, R. Chen, Y. Wang, and L. Chen, "Experimental study on corrosion of anchored rock mass for half-through intermittent joints," *Advances in Civil Engineering*, vol. 2019, Article ID 6018678, 12 pages, 2019.

[29] S. Wu, H. Chen, H. Lamei Ramandi et al., "Investigation of cable bolts for stress corrosion cracking failure," *Construction and Building Materials*, vol. 187, pp. 1224–1231, 2018.

[30] G. Grasselli, "3D behaviour of bolted rock joints: experimental and numerical study," *International Journal of Rock Mechanics and Mining Sciences*, vol. 42, no. 1, pp. 13–24, 2005.

[31] K. Spang and P. Egger, "Action of fully-grouted bolts in jointed rock and factors of influence," *Rock Mechanics and Rock Engineering*, vol. 23, no. 3, pp. 201–229, 1990.

[32] J.-T. Wen, W.-S. Zhu, and S.-C. Li, "Research on anchoring and shearing effect of anchoring cable," *Chinese Journal of Rock Mechanics and Engineering*, vol. 22, no. 10, pp. 1699–1703, 2003.

[33] X.-R. Ge and J.-W. Liu, "Study on shear behavior of anchored joint surface," *Chinese Journal of Geotechnical Engineering*, vol. 10, no. 1, pp. 8–19, 1988.

[34] S.-Q. Yang, Y.-H. Dai, L. Han, Y. He, and Y. Li, "Uniaxial compression experimental research on deformation and failure properties of brittle marble specimen with pre-existing fissures," *Chinese Journal of Rock Mechanics and Engineering*, vol. 12, pp. 2391–2404, 2009.

[35] T. Liu and R. W. Weyers, "Modeling the dynamic corrosion process in chloride contaminated concrete structures," *Cement and Concrete Research*, vol. 28, no. 3, pp. 365–379, 1988.

[36] Y.-S. Yuan, Y.-S. Ji, and Y.-J. Mou, "Propagation and model of distribution for corrosion of steel bars in concrete," *China Civil Engineering Journal*, vol. 40, no. 7, pp. 5–10, 2007.

[37] Y.-S. Ji, B.-Y. Zhang, L.-L. Zhang, H.-R. Ma, and P. Zeng, "Propagation of the corrosion layer and model of corrosion distribution on steel re-enforcing bar in concrete," *Journal of China University of Mining & Technology*, vol. 41, no. 3, pp. 355–360, 2012.

[38] Y.-L. Xu, "Analytical study on bond-anchorage between bar and concrete," *Building Science*, vol. 4, pp. 18–30, 1992.